Imaging-Guided pH-Sensitive Photodynamic Therapy Using Charge Reversible Upconversion Nanoparticles under Near-Infrared Light

*Chao Wang, Liang Cheng, Yumeng Liu, Xiaojing Wang, Xinxing Ma, Zhaoyi Deng, Yonggang Li, and Zhuang Liu**

Photodynamic therapy (PDT) based on upconversion nanoparticles (UCNPs) can effectively destroy cancer cells under tissue-penetrating near-infrared light (NIR) light. Herein, we synthesize manganese (Mn^{2+})-doped UCNPs with strong red light emission at ca. 660 nm under 980 nm NIR excitation to activate Chlorin e6 (Ce6), producing singlet oxygen ($^1O_2$) to kill cancer cells. A layer-by-layer (LbL) self-assembly strategy is employed to load multiple layers of Ce6 conjugated polymers onto UCNPs via electrostatic interactions. UCNPs with two layers of Ce6 loading (UCNP@2xCe6) are found to be optimal in terms of Ce6 loading and $^1O_2$ generation. By further coating UCNP@2xCe6 with an outer layer of charge-reversible polymer containing dimethylmaleic acid (DMMA) groups and polyethylene glycol (PEG) chains, we obtain a UCNP@2xCe6-DMMA-PEG nanocomplex, the surface of which is negatively charged and PEG coated under pH 7.4; this could be converted to have a positively charged naked surface at pH 6.8, significantly enhancing cell internalization of nanoparticles and increasing in vitro NIR-induced PDT efficacy. We then utilize the intrinsic optical and paramagnetic properties of Mn^{2+}-doped UCNPs for in vivo dual modal imaging, and uncover an enhanced retention of UCNP@2xCe6-DMMA-PEG inside the tumor after intratumoral injection, owing to the slightly acidic tumor microenvironment. Consequently, a significantly improved in vivo PDT therapeutic effect is achieved using our charge-reversible UCNP@2xCe6-DMMA-PEG nanoparticles. Finally, we further demonstrate the remarkably enhanced tumor-homing of these pH-responsive charge-switchable nanoparticles in comparison to a control counterpart without pH sensitivity after systemic intravenous injection. Our results suggest that UCNPs with finely designed surface coatings could serve as smart pH-responsive PDT agents promising in cancer theranostics.

1. Introduction

Photodynamic therapy (PDT) is a treatment strategy which uses photosensitizer (PS) molecules and light for cancer treatment. Upon irradiation of light with the appropriate wavelength, PS molecules can produce cytotoxic reactive oxygen species (ROS) and singlet oxygen ($^1O_2$) to destroy nearby cancer cells.[1,2] One of the greatest advantages of PDT is the ability to selectively treat the lesion area under light irradiation, while leaving normal tissues untouched. However, most PS molecules are excited by visible or even UV light, which have poor tissue-penetration capacity,[3] thus limiting the application of PDT in the treatment of large or internal tumors.

Recently, lanthanide ion-doped upconversion nanoparticles (UCNPs) have received much attention in biomedicine.[4–18] Compare with conventional fluorescent imaging based on energy down-conversion, photon upconversion (UC) is a process in which the sequential absorption of two or more near-infrared (NIR) photons leads to the emission of a single high-energy photon at the shorter wavelength, and thus shows significantly reduced autofluorescence background, improved tissue penetration depth, and lower phototoxicity during imaging.[3,14,19–22] Due to their

C. Wang, Dr. L. Cheng, X. Wang, Prof. Z. Liu
Jiangsu Key Laboratory for Carbon-Based Functional Materials & Devices
Institute of Functional Nano & Soft Materials (FUNSOM)
Soochow University
Suzhou, Jiangsu 215123, PR China
E-mail: zliu@suda.edu.cn

Y. Liu, X. Ma, Dr. Y. Li
Department of Radiology
The First Affiliated Hospital of Soochow University
Suzhou, Jiangsu, 215006, PR China

Z. Deng
Department of Earth and Space Science
University of Science and Technology of China
Hefei, Anhui, 230026, PR China

DOI: 10.1002/adfm.201202992

ability to convert NIR light into visible photons, UCNPs have also shown great promise in NIR light-induced PDT cancer treatment.[14,23–28] In several pioneering studies, it has been showed that $NaYF_4$:Yb,Er UCNPs coated with mesoporous silica containing PS molecules were able to produce single oxygen upon NIR irradiation with 980 nm light via resonance energy transfer for PDT cancer-cell killing.[23,25,27,29] In our recent work, we further realized highly effective NIR light-induced in vivo PDT treatment of cancer in mice by using Chlorin e6 (Ce6) adsorbed UCNPs.[24] It was found that the UCNP-based PDT induced by NIR light exhibited terrifically improved tissue penetration depth compared to traditional PDT using visible light.[24] Magnetic resonance (MR) imaging-guided PDT using UCNP-PS composites was subsequently demonstrated in vitro and in vivo by several other groups.[18,28] A few recent reports have also achieved in vivo PDT treatment of cancer upon systemic administration of UCNP-PS nanocomplexes.[27,28] Further efforts, however, are still demanded to develop smart UCNP-based PDT theranostic agents for environmentally controlled treatment as well as imaging-guided cancer therapy.

As the tumor extracellular environment is more acidic (pH 6.5–6.8) than blood and normal tissues (pH ca. 7.4), tremendous efforts have been devoted to develop various pH-responsive delivery vehicles for pH-triggered drug delivery and release.[30–36] In particular, one design strategy is to use charge-switching nanoparticles, which are negatively charged in neutral and alkaline environments but that switch to being positively charged under slightly acidic conditions, facilitating their interaction with negatively charged cell membranes to enhance cellular uptake of nanoparticles. Recently, Wang et al. described the use of 2,3-dimethylmaleic anhydride (DMMA) to obtain a pH-dependent charge-switchable polymer as an anticancer drug carrier.[30,33,35] In another work, Farokhzad et al. coated nanoparticles with poly(L-histidine), whose charges were also responsive to pH, for the treatment of bacterial infections.[31]

In this study, we for the first time realize pH-responsive PDT using PS molecules loaded with charge-reversible UCNPs, for dual-modal imaging-guided NIR-excited PDT cancer treatment. **Figure 1**A gives a schematic illustration of the fabrication process. Single-band red-emitting UCNPs based on Mn^{2+}-doped $NaYF_4$:Yb,Er (Y:Mn:Yb:Er = 50:30:18:2) are synthesized. A layer-by-layer (LBL) self-assembly process is carried out to load multiple layers of PS molecules and Ce6 onto UCNPs. The obtained nanoparticles with a double-layered Ce6 coating (UCNP@2xCe6) are further covered with a pH-responsive polyethylene glycol (PEG) grafted polymer containing DMMA groups, yielding UCNP@2xCe6-DMMA-PEG, the charge of which is highly sensitive to the environmental pH. Utilizing the intrinsic optical and paramagnetic properties of Mn-doped UCNPs, we are able to track their behaviors in vitro and in vivo by dual modal upconversion luminescence (UCL) and MR imaging. It is found that UCNP@2xCe6-DMMA-PEG shows remarkably increased in vitro intracellular uptake under acidic cell culture at pH 6.8 and, more interestingly, obviously enhanced in vivo tumor retention after either intratumor injection or intravenous (i.v.) administration, owing to the slightly acidic tumor microenvironment. As the results, both in vitro and in vivo experiments evidence improved PDT cancer killing efficacy under NIR light exposure using our charge-reversible nanoparticles. Our work demonstrates a design of a smart UCNP-based theranostic agent that enables dual-model imaging-guided, pH-sensitive, NIR light-induced phototherapy of cancer.

2. Results and Discussion

In our previous study, we demonstrated in vivo PDT based on UCNP-Ce6 complex.[24] However, $NaYF_4$:Yb,Er-based UCNPs usually give a bright green emission (around 550 nm) and a weaker red emission (around 660 nm). In our previous UCNP-Ce6 system, only the relatively weak red emission was used to excite Ce6 molecules adsorbed on nanoparticles, while the strong green emission was not utilized in energy transfer (see the Supporting Information, SI, Figure S1). To address this problem, we synthesized single-band upconversion emitting UCNPs with intense red light (650–670 nm) luminescence by manganese (Mn^{2+}) doping using a solvothermal method.[37] Our synthesized Mn^{2+}-doped UCNPs exhibited uniform sizes with an average diameter of around 20 nm, as shown by the transmission electron microscopy image (Figure 1B). High-resolution TEM showed the lattice fringes with an observed *d*-spacing of 0.292 nm, which is in good agreement with the lattice spacing in the (101) planes of cubic $NaYF_4$ (Figure 1B). Energy-dispersive X-ray (EDX) analysis of individual nanocrystals evidenced the existence of manganese ions in our UCNPs (see the SI, Figure S2).[37] The X-ray diffraction pattern (XRD) of NaY(Mn)F_4:Yb, Er samples could be ascribed to a mixture of the cubic (JDPDS. 06-342) and hexagonal (JCPDS. 16-334) phases, with the former as the dominant phase (see the SI, Figure S3).

To make Mn^{2+}-doped UCNP water soluble, hydrophobic ligands on the surface of as-prepared nanoparticles were replaced through a ligand exchange reaction by polyacrylic acid (PAA).[38] Different from $NaYF_4$:Yb,Er-based UCNPs, our Mn^{2+}-doped UCNPs with PAA coating (UCNP/PAA) in the aqueous solution gave a strong single emission peak around 660 nm (Figure 1C and S1, in the SI). Previous reports have evidenced that manganese ions (Mn^{2+}) could be used as a T_1 contrast agent in MR imaging.[39,40] In our study, an obvious concentration-dependent brightening effect was observed in T_1-weighted MR images (Figure 1D), showing a transverse relaxivity (r_1) of 7.08 S^{-1} mM^{-1} on the basis of the Mn concentration, and a r_2/r_1 value of 3.72 (Figure 1E and S4, in the SI).

In our earlier work, Ce6 was adsorbed on the surface of UCNPs by the hydrophobic interaction, which was a relatively weak force and could result in the gradual detachment of Ce6 molecules from nanoparticles. In this study, Ce6 loading on UCNPs was realized by the LbL process (Figure 1A). To synthesize Ce6-conjugated polymer, a small percentage of amino groups (approximately 7.1%) in poly(allylamine hydrochloride) (PAH) after deprotonation was conjugated to Ce6, while the leftover amino groups were blocked by succinic anhydride (SA), forming a negatively charged PAH-Ce6-SA polymer (see the SI, Figures S5–S8). To load Ce6 on UCNPs, UCNP/PAA was first mixed with oppositely charged PAH to form positively charged UCNP/PAA/PAH, on which the counter-polyelectrolyte PAH-Ce6-SA was adsorbed (see the SI, Figure S9). The

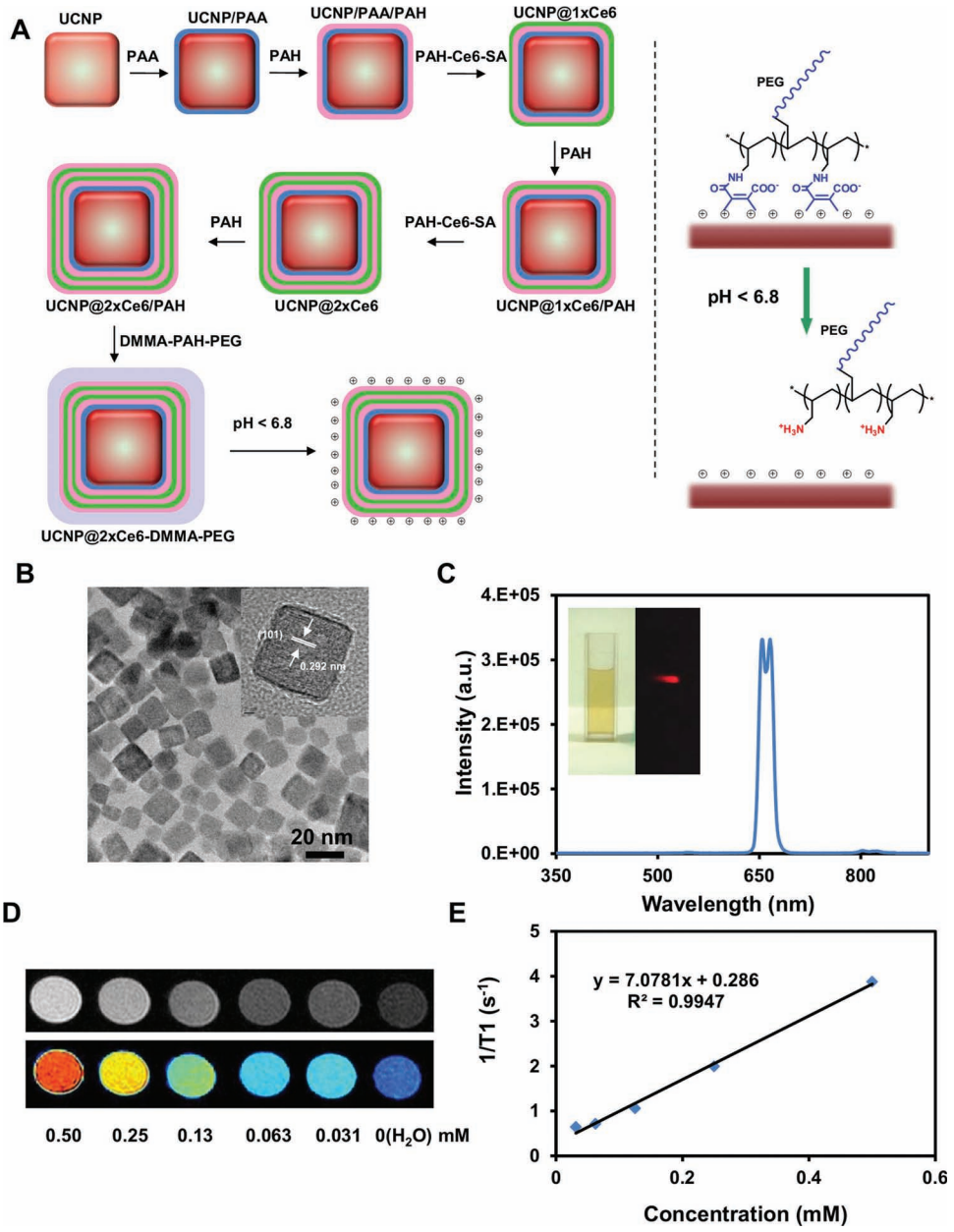

Figure 1. Schematic illustration and characterization of pH-responsive smart theranostic UCNPs. A) A schematic showing the fabrication process of pH-sensitive charge-reversible UCNPs with multi-layers of Ce6 loading; left: the detachment of PAH-DMMA-PEG from the positively charged nanoparticle surface under pH 6.8. B)TEM micrograph of Mn^{2+}-doped UCNPs; inset: high-resolution TEM image of a UCNP. C) A UCL emission spectrum of Mn^{2+}-doped UCNPs under 980 nm laser excitation; inset: photo of a UCNP solution under ambient light and under 980 nm laser excitation. D)T_1-weighted MR images of UCNP solutions at different concentrations. E)T_1 relaxation rates (r_1) of UCNP solutions at different Mn^{2+} concentrations.

stepwise formation of PAH/PAH-Ce6-SA multilayer coatings on UCNPs was further carried out, obtaining UCNP@1xCe6, UCNP@2xCe6, and UCNP@3xCe6, with one, two, and three layers of PAH/PAH-Ce6-SA coatings, respectively. Dynamic light scattering (DLS) analysis of UCNP@*n*xCe6 multilayer-coated nanoparticles (n = 0, 1, 2, 3) revealed their particle sizes to be appropriately 50, 59, 80, and 140 nm, respectively (**Figure 2**A). Meanwhile, UCNPs coated with various numbers of polymer layers showed discrete zeta potentials alternating between positive and negative (Figure 2B). This observation indicated the successful LbL assembly of charged polymers on nanoparticles. The UCNP@*n*xCe6 multilayer NPs were also characterized by UV-Vis and UCL spectra (Figure 2C). The Ce6 absorbance peak at 660 nm increased with the number of PAH/PAH-Ce6-SA layers, suggesting the increased Ce6 loading. On the other hand, we observed an obvious decline in UCL emission at ca. 660nm owing to the resonance energy transfer from UCNPs to Ce6. The loading capacity of Ce6 onto UCNPs

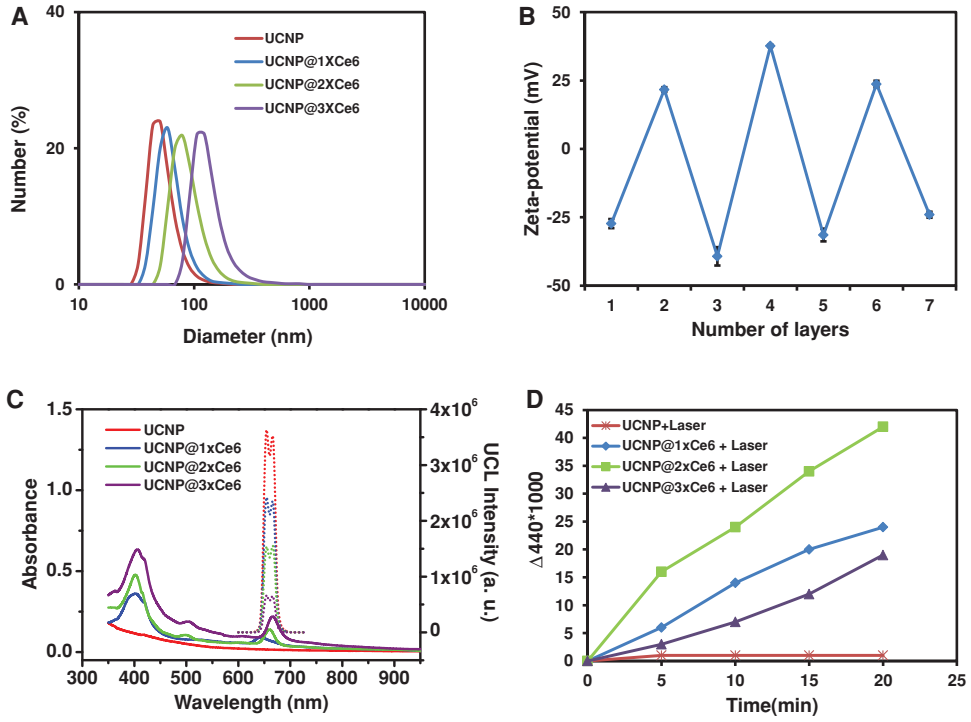

Figure 2. Characterization of UCNP nanocomplexes with different layers of Ce6 loading. A) DLS data of UCNP@*n*xCe6 with multiple layers of polymer coatings (n = 0, 1, 2, 3). B) Zeta potentials of UCNPs coated with increasing numbers of polymer coating layers: 1) UCNP/PAA, 2) UCNP/PAA/PAH, 3) UCNP@1xCe6, 4) UCNP@1xCe6/PAH, 5) UCNP@2xCe6, 6) UCNP@2xCe6/PAH, and, 7) UCNP@3xCe6. C) UV-Vis and UCL spectra of UCNP@*n*xCe6 (n = 0, 1, 2, 3) nanocomplexes. D) Singlet oxygen generation by UCNP@*n*xCe6 (n = 0, 1, 2, 3) nanocomplexes under 980 nm laser irradiation. The UCNP concentration was the same (0.5 mg mL^{-1}) for different UCNP@*n*xCe6 (n = 0, 1, 2, 3) nanocomplexes in (C) and (D).

were determined to be 3.4%, 7.7%, and 11.0% (w/w), for UCNP@1xCe6, UCNP@2xCe6, and UCNP@3xCe6, respectively. It is worth noting that this strategy leaded to a tight coupling between PS molecules and UCNPs, and hardly any Ce6 was found to be released from UCNPs within 2 d under physiological conditions (see the SI, Figure S10).

We next studied the singlet oxygen generation of our UCNP@*n*xCe6 complexes by measuring the bleaching of *N,N*-dimethyl-4-nitrosoaniline (RNO), whose absorbance at 440 nm would be diminished in the presence of $^1O_2$. It was found that at the same UCNP concentration, UCNP@2xCe6 showed the highest efficiency in terms of $^1O_2$ production under 980 nm laser irradiation (Figure 2D). Increasing the number of PAH/PAH-Ce6-SA layers to 3 resulted in reduced $^1O_2$ production, likely due to the significant self-quenching between Ce6 molecules when too many Ce6 molecules were packed closely together. The fluorescence of Ce6 from different UCNP@*n*xCe6 complexes revealed a similar trend (see the SI, Figure S11). We thus chose UCNP@2xCe6 for further study.

To offer UCNPs pH-responsive charge reversibility, we synthesized a pH-sensitive polymer by co-grafting deprotonated PAH with PEG (approximately 10% of amino groups) and DMMA (the leftover amino groups), and obtained a negatively charged PAH-DMMA-PEG (see the SI, Figure S5), which was used to coat UCNP@2xCe6/PAH by electrostatic interactions, affording UCNP@2xCe6-DMMA-PEG with excellent stability in various physiological solutions (see the SI, Figure S12). Previous studies have demonstrated that the amide bond formed between the amino group and DMMA could be cleaved under slightly acidic conditions. In our study, obvious charge conversion, with the nanoparticle zeta potential increasing from around –18 to +10 mV in approximately 2 h, was observed for UCNP@2xCe6-DMMA-PEG at pH 6.8, which was close to the tumor extracellular environmental pH (**Figure 3**A). While at normal physiological pH (7.4), the nanoparticle zeta potential remained negative over 4 h. As a control, we synthesized another polymer by replacing DMMA with succinic anhydride (SA), and obtained PAH-SA-PEG (se the SI, Figure S5) without charge reversibility to functionalize Ce6-loaded UCNPs. As expected, we found that UCNP@2xCe6-SA-PEG was not sensitive to the change of pH, showing stable negative zeta potentials (ca. –20mV) at either pH 7.4 or 6.8 (Figure 3A). The hydrodynamic diameters of UCNP@2xCe6-DMMA-PEG and UCNP@2xCe6-SA-PEG under different pHs were measured by DLS over time (see the SI, Figure S13). A significant decrease of nanoparticle diameter was noted for UCNP@2xCe6-DMMA-PEG under pH 6.8, but not for the same sample under pH 7.4, indicating the acid-induced detaching of PEG coating in this nanocomplex. In contrast, the DLS measured diameters of UCNP@2xCe6-SA-PEG were not sensitive to pH and kept at constant levels under both pHs.

To further demonstrate whether UCNP@2xCe6-DMMA-PEG could be more efficiently internalized by cancer cells at the lower pH, we incubated UCNP@2xCe6-DMMA-PEG

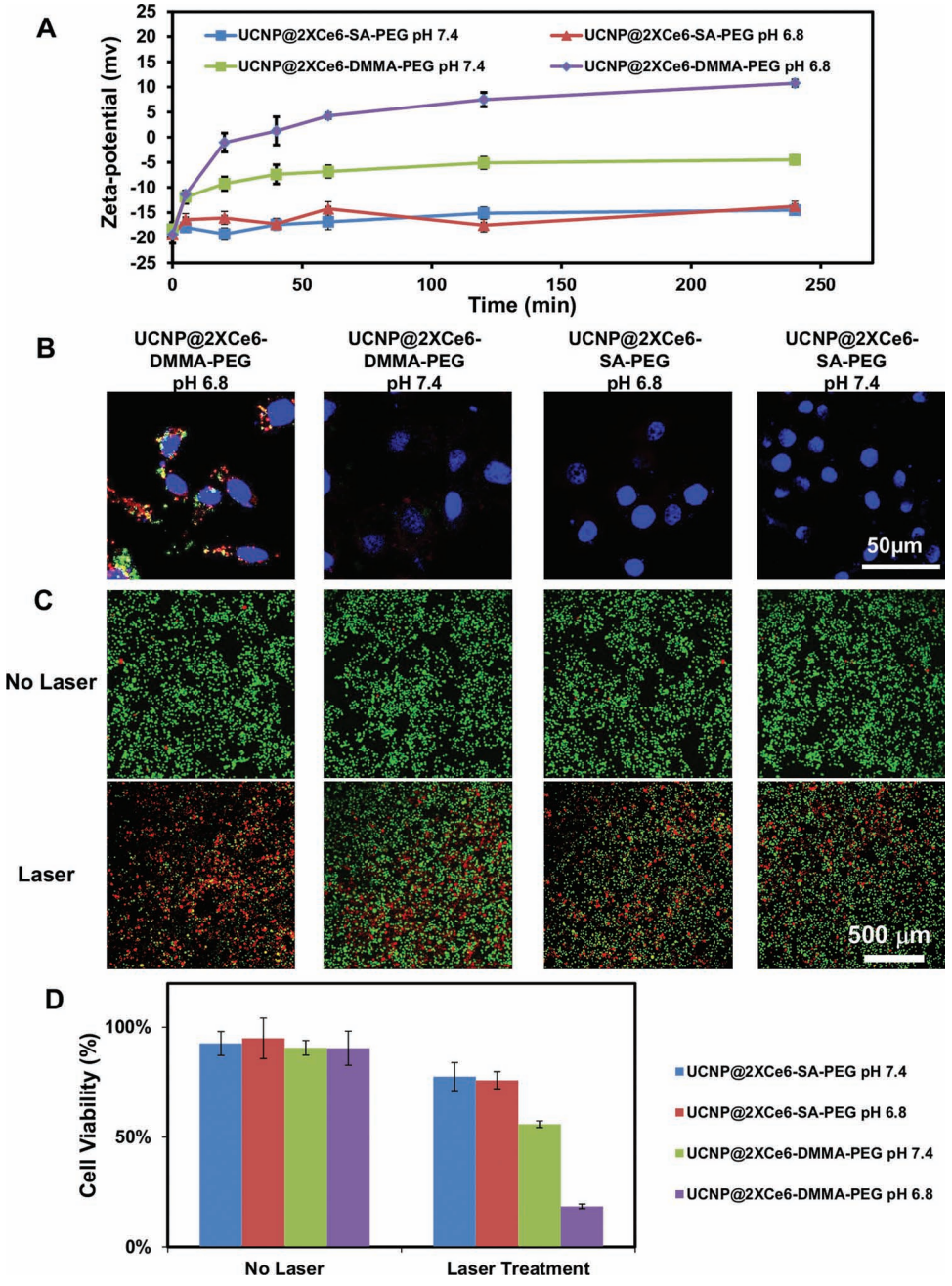

Figure 3. pH-induced charge conversion of our smart nanoparticles. A) Zeta potential changes of UCNP@2xCe6-DMMA-PEG and UCNP@2xCe6-SA-PEG after incubation at pH 7.4 or 6.8 for different periods of time. B) Confocal laser scanning microscopy imaging of HeLa cells after being incubated with UCNP@2xCe6-DMMA-PEG or UCNP@2xCe6-SA-PEG at pH 6.8 or 7.4 for 2 h. Green: the UCL emission from UCNPs; Red: Ce6 fluorescence; Blue: DAPI (nuclear staining). C) Confocal images of Calcein AM/PI co-stained cells after being incubated with UCNP@2xCe6-DMMA-PEG or UCNP@2xCe6-SA-PEG for 4 h, with or without 980 nm laser irradiation. Live and dead cells were stained green and red, by Calcein AM and PI, respectively. D) Cell viability data of HeLa cells after various treatments indicated with and without the 980 nm laser irradiation as evaluated by the standard MTT Assay. Error bars are based on four parallel samples.

or UCNP@2xCe6-SA-PEG with HeLa cells at pH 7.4 or 6.8 for 2 h. From confocal laser scanning microscopy imaging (Figure 3B), we observed much stronger UCL signals together with largely co-localized Ce6 fluorescence inside cells incubated with UCNP@2xCe6-DMMA-PEG at pH 6.8, compared to those incubated with identical nanoparticles at pH 7.4. Little signal could be observed from cells incubated with UCNP@2xCe6-SA-PEG at either pH. This observation suggested that our pH-responsive nanoparticles exhibited significantly enhanced cellular internalization at slightly acidic pH due to their charge conversion from negative to positive.

We then used UCNP@2xCe6-DMMA as a pH-responsive PDT agent in cancer therapy in cell experiments. UCNP@2xCe6-DMMA-PEG or UCNP@2xCe6-SA-PEG was incubated with

HeLa cells for 4 h. After the incubation, cells were washed with phosphate buffer saline (PBS) to remove free nanoparticles, and then exposed to a 980 nm NIR laser at a power density of 0.4 W cm^{-2}. Calcein-AM/propidium iodide (PI) double staining was carried out to differentiate live and dead cells under confocal fluorescence microscope (Figure 3C). Without laser irradiation, most cells remained alive after being treated with nanocomplexes at different pHs. Significantly increased cell death was observed for cancer cells incubated with UCNP@2xCe6-DMMA-PEG at pH 6.8 for 4 h and exposed to the NIR light, in marked contrast to those cells after the same treatment but incubated at the normal pH (7.4; Figure 3C). The cell death was insignificant for those incubated with UCNP@2xCe6-SA-PEG at either pH 6.8 or 7.4 after laser exposure (Figure 3C). Quantitative cell viability data further confirmed the pH-responsive PDT cancer cell killing using our UCNP@2xCe6-DMMA-PEG (Figure 3D).

To further explore the potential of charge-reversible UCNP@2xCe6-DMMA-PEG for in vivo cancer therapy, intratumoral (i.t.) injection of UCNP@2xCe6-DMMA-PEG into 4T1 murine breast cancer tumor bearing Balb/c mice was carried out. As shown in **Figure 4**A and B, when injected with these two different types of nanoparticles, obviously UCL emission and T_1-weighted MR signals were observed from tumors on mice. However, after 1 d, both MR and UCL intensities sharply decreased for the mice injected with UCNP@2xCe6-SA-PEG, while only a slight decline was found for the mice injected with UCNP@2xCe6-DMMA-PEG. Quantitative data analysis indicated that UCNP@2xCe6-DMMA-PEG was retained at the tumor site for much longer compared with UCNP@2xCe6-SA-PEG (Figure 4C and D). Due to the slightly acidic tumor pH, the initial negative UCNP@2xCe6-DMMA-PEG nanoparticles in the tumor could be converted into positively charged nanoparticles without PEG coating (Figure 1A), which exhibit strong binding to negative membranes of cancer cells and tumor tissues. While for UCNP@2xCe6-SA-PEG without charge reversibility, those negatively charged and PEG coated nanoparticles may be less 'sticky' and could be cleared out from the tumor by blood and/or lymphatic circulation.

We next evaluated the in vivo antitumor therapeutic efficacy of our pH-responsive UCNP@2xCe6-DMMA-PEG in a 4T1 murine breast tumor mouse model. 4T1 tumor-bearing Balb/c mice were i.t. injected with UCNP@2xCe6-DMMA-PEG or UCNP@2xCe6-SA-PEG at the same dose of ca. 0.4 mg (in terms of UCNP weight) per mouse. On day 1 post-injection of nanoparticles, the mice were exposed to 980 nm NIR laser at a power density of 0.5 W cm^{-2} for 30 min (900 J cm^{-2}), with 1 min intervals every 1 min to avoid any tissue damage by heating. Saline-injected mice and non-irradiated mice were used as controls. Seven mice were used in each group. As shown in Figure 4E, neither nanoparticle injection by itself nor NIR-laser irradiation alone was able to delay the tumor growth. Although the tumor growth was retarded in both UCNP@2xCe6-DMMA-PEG and UCNP@2xCe6-SA-PEG treated groups with laser irradiation, the former with the charge-reversibility showed significantly higher anti-tumor efficacy, owing to the enhanced retention of those nanoparticles in acidic tumor micro-environment (Figure 4D).

Finally, we examined the potential of UCNP-DMMA-PEG for in vivo tumor acidity-targeting based on systemic adminstration. Both UCNP-DMMA-PEG and UCNP-SA-PEG (without Ce6 loading) at the same concentration were i.v. injected into mice bearing 4T1 tumors. As shown in **Figure 5**A and B, strong UCL signals were observed in the tumors of mice after i.v. injection of UCNP-DMMA-PEG, suggesting high tumor uptake of those charge-reversible UCNPs, whereas mice injected with UCNP-SA-PEG showed rather lower tumor accumulation of nanoparticles. Quantification of UCL signals from tumors showed that the tumor uptake of UCNP-DMMA-PEG was 6.4-fold more efficient compared to that of UCNP-SA-PEG, at 2 h post-i.v. injection (Figure 5C and D). Confocal images of tumor slices also confirmed a significantly increased tumor uptake of UCNPs with charge reversibility. Therefore, it is likely that those pH-responsive charge-reversible UCNPs could be converted from negatively charged nanoparticles with PEG coating when circulating in the blood, into positively charged 'naked' nanoparticles inside the acidic tumor microenvironment, thus exhibiting greatly enhanced tumor retention.

Despite this greatly increased tumor accumulation of UCNPs via coating them with pH-sensitive charge-reversible polymers, we found that the majority of injected UCNPs were still accumulated in reticuloendothelial systems (RES), such as the liver and spleen, after systemic administration (see the SI, Figure S14). Unfortunately, the in vivo PDT cancer-treatment efficacy of UCNP@2xCe6-DMMA-PEG after i.v. injection was still unsatisfactory in our pilot study, likely due to the fact that the current tumor uptake of nanoparticles was still not high enough to render significant therapeutic effect under PDT. Further development of smart UCNP-PS complexes with better surface functionalization to enhance their tumor targeting as well reduce their RES retention is still being studied in our laboratory.

3. Conclusions

We successfully developed charge-reversible UCNPs for pH-sensitive in vivo PDT, which could be guided by UCL and MR dual-modal imaging. Via an LbL self-assembly approach, we fabricate Ce6 loaded UCNPs which are coated with a pH-sensitive polymer. While stable under normal physiological pH at 7.4, highly sensitive pH-induced charge conversion of those UCNP@2xCe6-DMMA-PEG nanoparticles is observed in slightly acidic environment, under which conditions significantly enhanced cellular internalization of nanoparticles and remarkably improved cancer-cell killing efficacy are realized. We further utilized the intrinsic optical and paramagnetic properties of Mn^{2+}-doped UCNPs for in vivo dual modal imaging, and uncovered the enhanced retention of UCNP@2xCe6-DMMA-PEG inside the tumor after i.t. injection, owing to the slightly acidic tumor microenvironment. A significantly improved in vivo PDT therapeutic effect was then achieved using our charge-reversible UCNP@2xCe6-DMMA-PEG nanoparticles. Finally, we further uncovered greatly increased tumor accumulation of pH-responsive charge-reversible UCNP-DMMA-PEG after i.v. injection, suggesting the potential of tumor acidity-targeted in vivo imaging and therapy using environmentally responsive nano-agents.

Our work presents an interesting and easy strategy to stably load therapeutic agents, PS molecules in this case, on UCNPs

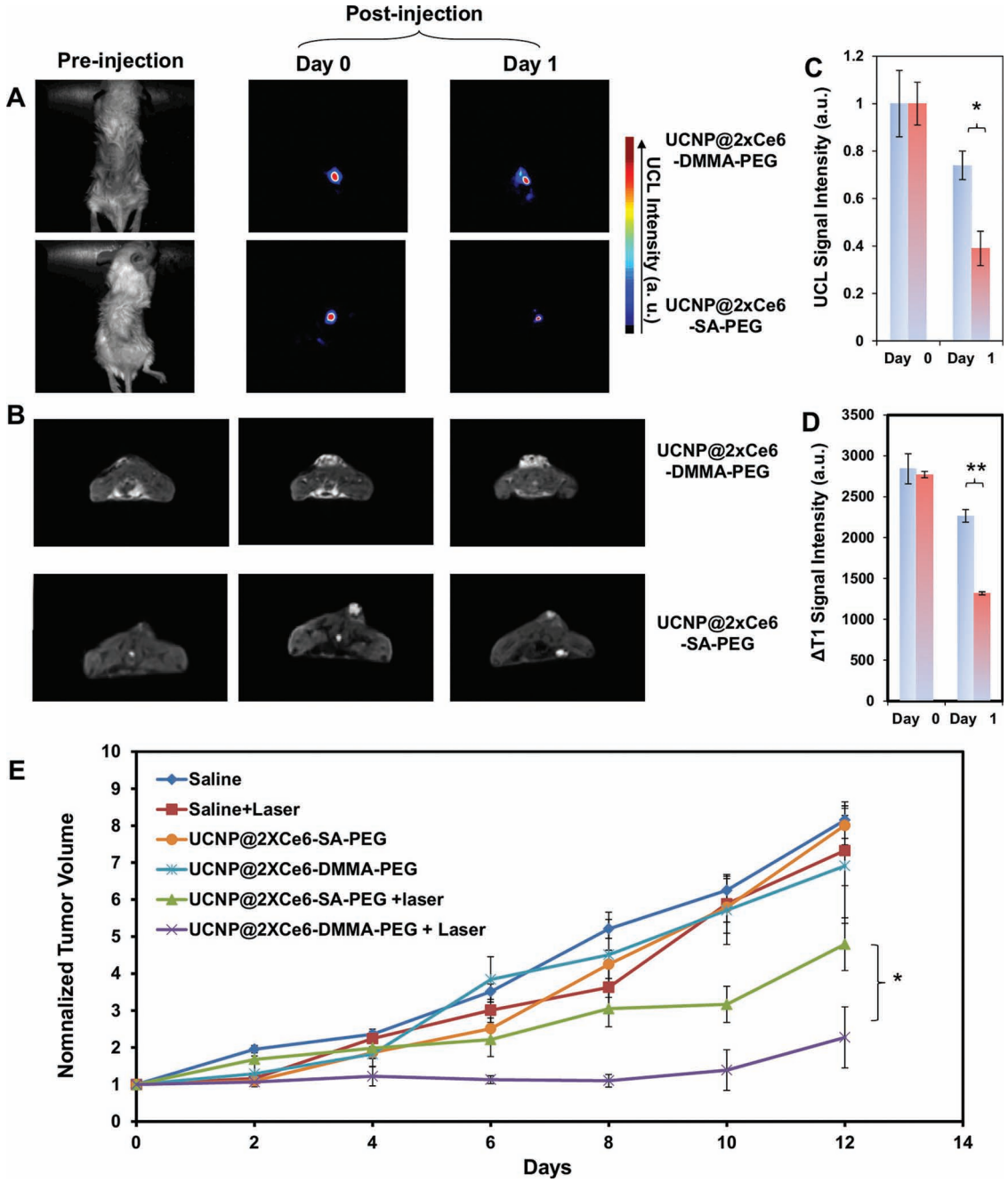

Figure 4. In vivo dual modal imaging-guided PDT. A,B) In vivo UCL images (A) and T_1 MR images (B) of mice after intratumoral injection with UCNP@2xCe6-DMMA-PEG or UCNP@2xCe6-SA-PEG. The images were taken at different times post-injection. C,D) Quantification of UCL intensities (C) and increased T_1 MR signals as presented by ΔT_1 versus un-injected tumor (D) from the tumor side at different times post-injection of UCNP@2xCe6-DMMA-PEG (blue) or UCNP@2xCe6-SA-PEG (red). Error bars are based on three mice per group. E)Tumor growth curves of different groups of mice after various treatments, as indicated. Error bars are based on seven mice per group. *P*-values are calculated based on Student's *t*-test, with ** < 0.01, and * < 0.05.

via the LbL method, which could be easily extended to the surface engineering of other nanomaterials for controllable molecular loading and release. The pH-sensitive nano-interface chemistry developed in this work is also a rather simple and versatile strategy applicable to a wide variety of functional nanomaterials for pH-responsive biomedical imaging and therapy. Last but not least, this work is the first time to demonstrate multimodal imaging-guided, pH-sensitive, NIR-induced photodynamic therapy using UCNPs as a smart agent, which is promising for future applications in cancer theranostics.

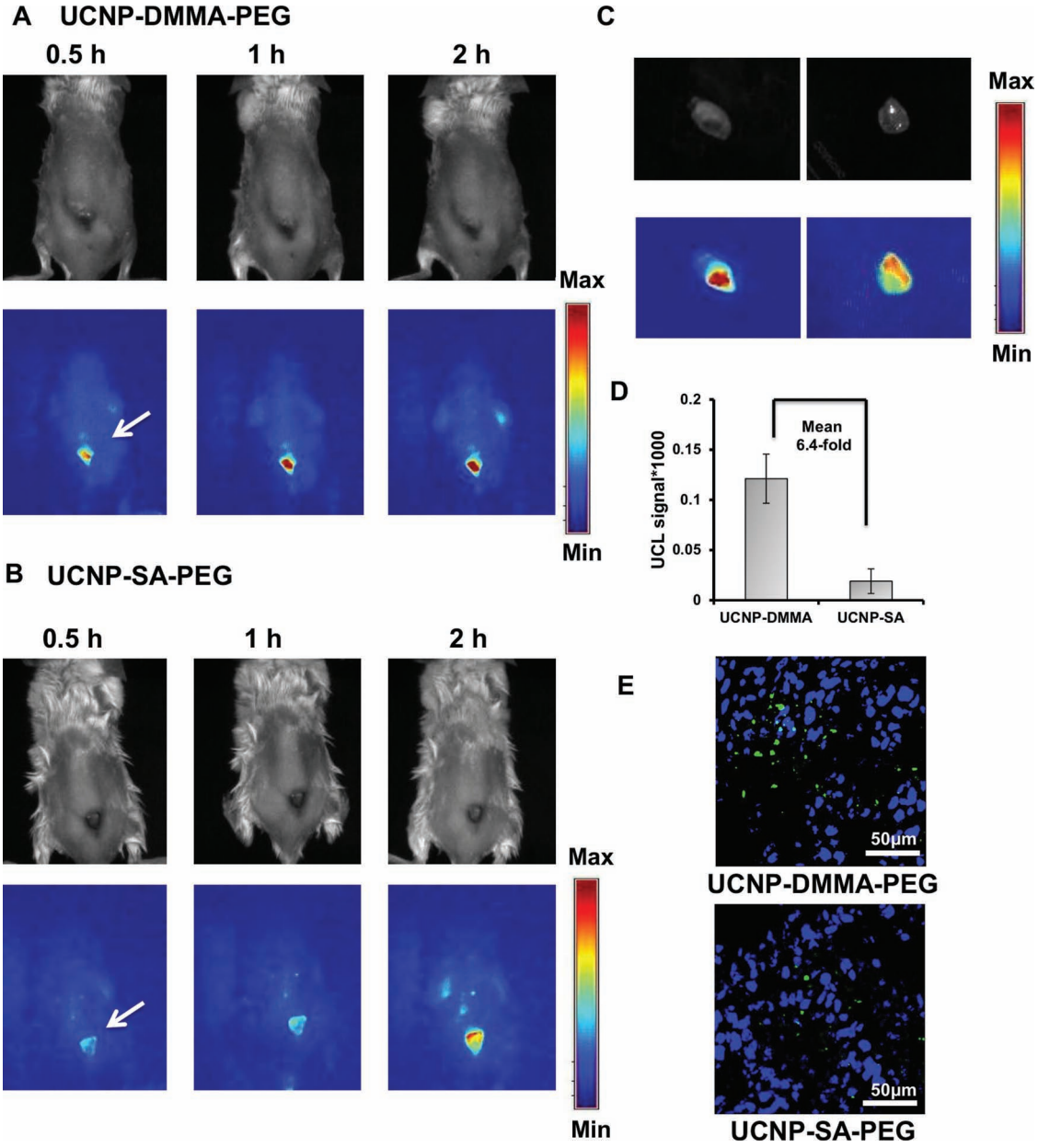

Figure 5. Tumor targeting of pH-responsive nanoparticles after systemic administration. A,B) UCL images of babl/c mice after intravenous injection of UCNP-DMMA-PEG (A) or UCNP-SA-PEG (B) at the same UCNP dose. Images were taken at different time points post-injection. Arrows indicate tumor sites. The top row shows bright-field images and the bottom row pseudo-colored UCL images. All images in (A) and (B) are presented under the same intensity scale. C)Ex vivo UCL imaging of tumors taken 2 h after i.v. injection of UCNP-DMMA-PEG or UCNP-SA-PEG. D) Quantification of tumor UCL signals. Error bars are based on three mice per group. E) Confocal images of tumor slices taken from mice as showed in (C), where green and blue represent UCL and DAPI signals (cell nuclei), respectively.

4. Experimental Section

Materials: All chemicals, unless specified otherwise, were purchased from Sigma-Aldrich and used as received. PEG polymers were purchased from PegBio, Suzhou, China. All cell-culture related reagents were purchased from Hyclone.

Instrumentation: Zeta potential and DLS measurements were carried out on a nanoparticle analyzer Nano-ZS90 (Malvern Instruments Ltd). Infrared spectra were recorded using VERTEX 70/70v FT-IR spectrometers. TEM images were taken by a Tecnai G2F20 transmission electron microscope (FEI Company). Powder X-ray diffraction was recorded on PANalytical XRD diffractometer using Cu-Ka radiation. UV-vis absorption spectra were recorded with a PerkinElmer UV-Vis spectrophotometer. Fluorescent emission spectra were measured on a FluoroMax-4 luminescent spectrometer (HORIBA JobinYvon S.A.S) using either a xeon lamp or a 980 nm laser diode as the excitation source.

Synthesis of UCNPs: Mn^{2+} ion-doped $NaY(Mn)F_4$:Yb/Er nanocrystals (Y:Mn:Yb:Er = 50:30:18:2) were prepared as reported previously.[37] In brief, 1.2 mL of 0.5 M $MnCl_2$, 2 mL of 0.5 M $Y(NO_3)_3$, 1.8 mL of 0.2 M $Yb(NO_3)_3$, and 0.2 mL of 0.2 M $Er(NO_3)_3$ were added to a mixture of

NaOH (0.6 g), deionized water (3.0 mL), oleic acid (10 mL) and ethanol (20 mL) under stirring. 4 mL of deionized water containing 8 mmol of NaF was then dropwisely added into the mixture. After vigorous stirring at room temperature for 15 min, the colloidal solution was transferred into a 60 mL Teflon-lined autoclave, which was sealed and heated at 200 °C for 8 h. The system was then allowed to cool naturally to room temperature. The final product was collected by centrifugation, and then washed with ethanol and deionized water several times to remove any possible remnants. The obtained UCNPs could be re-dispersed in various non-polar organic solvents.

Synthesis of PAA-UCNP: The PAA-UCNP synthesis was carried out following a literature protocol.[2] To a flask containing 30 mL diethylene glycol (DEG), 300 mg of PAA with a molecular weight (MW) at 1800 Da was added. The mixture was heated to 110 °C to form a clear solution. A toluene solution containing 100 mg OA-UCNP nanocrystals was slowly added. After maintaining the temperature at 110 °C for 1 h under argon protection, the solution was heated to 240 °C for 1.5 h. The resultant solution was cooled to room temperature. Ethanol was then added to yield a precipitate. The obtained UCNP/PAA were recovered via centrifugation and washed three times with ethanol/water (1:1 v/v).

Synthesis of Polymers: Deprotonation of PAH·HCl. PAH·HCl (374 mg) was mixed with NaOH (200 mg) in 5 mL water. The solution was dialyzed for 12 h against water using a dialysis membrane with a molecular weight cut-off (MWCO) of 3.5 kDa before being frozen dried, obtaining deprotonated PAH for further use.

Synthesis of PAH-PEG: 22.8 mg deprotonated PAH was reacted with 200 mg 5kDa mPEG-COOH (10% of amino groups in PAH were conjugated to PEG) in 5 mL anhydrous DMSO with the addition of 20 mg EDC and 15 µL triethylamine (TEA). The solution was reacted for 24 h at room temperature before being added into water, and then dialyzed using a dialysis membrane (MWCO = 12 kDa) for at least 36 h to remove excess reagents. The solution was freeze-dried and stored below –20 °C for further use. The actual PEGylation ratio on the PAH polymer was measured by NMR spectrum to be approximately 9.61%.

Synthesis of PAH-DMMA-PEG: 100 mg PAH-PEG was mixed with 40 mg dimethylmaleic anhydride (DMMA) and 50 µL TEA in 5 mL DMSO. After 24 h of reaction, the mixture was added into water and dialyzed against pH 8–9 water (adjusted by NaOH) for at least 36 h to remove excess DMMA (MWCO = 3.5 kDa). The solution was freeze-dried and stored below –20 °C for further use.

Synthesis of PAH-SA-PEG: 100 mg PAH-PEG was mixed with 33 mg succinic anhydride (SA) and 50 µL TEA in 5 mL DMSO. The mixture was added into water and dialyzed against pH 8–9 water (adjusted by NaOH) for at least 36 h to remove excess SA (MWCO = 3.5 kDa). The solution was freeze-dried and stored below –20 °C for further use.

Synthesis of PAH-CE6-SA: 25 mg Ce6 was activated by 8 mg EDC (1.0 eq) and 5 mg NHS (1.0 eq) in 5 mL anhydrous DMSO for 30 min. The activated Ce6-NHS was then added into 57 mg deprotonated PAH dissolved in DMSO. After 24 h of reaction, 150 mg SA was added into the reaction mixture together with 200 µL TEA to quench unreacted amino groups in PAH. After another 24 h of reaction, the mixture was added into water and dialyzed against distilled water for least 36 h (MWCO = 3.5 kDa). The final product was frozen dried and stored below –20 °C for further use. Based on the UV-VIS spectrum of the obtained PAH-Ce6-SA polymer, approximately 7.1% of amino groups on PAH were conjugated to Ce6.

Chlorin e6 Loading on UCNPs: First, 5 mL (0.5 mg mL^{-1}) of UCNP/PAA aqueous solution was dropwisely added into 5 mL of PAH aqueous solution (MW = 15 000, 1 mg mL^{-1}) under ultrasonication for 30 min using a ultrasonic-bath (KQ-100KDB, KunShan Ultrasonic Instruments Co., Ltd). After stirring for 6 h, a UCNP/PAA/PAH solution was obtained and purified by centrifugation (14 800 rpm for 10 min) to remove excess PAH. Second, the above UCNP/PAA/PAH solution was dropwisely added into 5 mL of PAH-Ce6-SA aqueous solution under ultrasonication for 30 min and then stirred for 6 h. The UCNP/PAA/PAH/PAH-Ce6-SA (UCNP@1xCe6) solution was obtained and purified by centrifugation (14 800 rpm for 10 min) to remove excess PAH-Ce6-SA. This procedure was repeated once or twice to acquire UCNP@2xCe6 and UCNP@3xCe6, respectively. Lastly, to prepare UCNP@2xCe6-DMMA-PEG or UCNP@2xCe6-SA-PEG, UCNP@2xCe6 was first coated with PAH and then dropwisely added into 5 mL of PAH-DMMA-PEG or PAH-SA-PEG aqueous solution, respectively, under ultrasonication for 30 min. After purification by centrifugation to remove excess coating polymers, the final products in aqueous solutions were stored under 4 °C for the future use.

Cellular Experiments: 4T1 murine breast cancer cells and HeLa human epithelial carcinoma cells were originally obtained from the American Type Culture Collection (ATCC) and cultured under the recommended conditions. Confocal luminescence imaging of cells was performed with a modified Laika laser-scanning microscope. The fluorescence of Ce6 (emission range 600 to 750 nm) and the UCL emission of UCNPs (emission range 600 to 700 nm) were excited by using a 633 nm laser and a 980 nm external laser, respectively. Cell nuclei were stained by 4′,6-diamidino-2-phenylindole (DAPI). The in vitro cytotoxicity was measured using a standard methyl thiazolyl tetrazolium (MTT, Sigma Aldrich) assay. HeLa cells were seeded into 96-well cell culture plates at 1×10^4 per well until adherent and then incubated with UCNP@2xCe6-DMMA-PEG or UCNP@2xCe6-SA-PEG at a concentration of 100 µg mL under pH 6.8 or 7.4 for 4 h. After removal of nanoparticles, cells were transferred into fresh media and irradiated by the 980 nm laser at a power density of 0.5 W cm^{-2} for 10 min (300 J cm^{-2}). The cells were then incubated at 37 °C for additional 48 h before the MTT assay to determine their viabilities relative to the control untreated cells.

Animal Model and in vivo PDT Treatment: Female Balb/c mice (weight = 20 g) were obtained from Suzhou Belda Bio-Pharmaceutical Co. and used under protocols approved by Soochow University Laboratory Animal Center. To generate the 4T1 murine breast tumor model, 5×10^6 4T1 cells in 20 µL serum-free RMPI-1640 medium were subcutaneously injected onto the back of each female Balb/c mouse. The mice were treated when the tumor volumes approached 40 to 50 mm^3. For the PDT treatment, each 4T1 tumor was intratumorally injected with ca. 40 µL saline, UCNP@2xCe6-DMMA-PEG, or UCNP@2xCe6-SA-PEG (10 mg mL^{-1} UCNPs). One day after injection, an optical fiber-coupled 980 nm diode laser (Hi-Tech Optoelectronics Co., Ltd. Beijing, China) was used to irradiate tumors at a power density of 0.5 W cm^{-2} for 30 min (ca. 900 J cm^{-2}) with a 1 min interval after each minute of irradiation to avoid significant tissue heating. The tumor sizes were measured by a caliper every other day and calculated as the volume V = (tumor length) × (tumor width)^2/ 2. Relative tumor volumes were calculated as V/V_0, where V_0 was the tumor volume when the treatment was initiated.

In vivo UCL&MR Imaging: A modified Maestro in vivo imaging system using a 980 nm optical fiber coupled laser as the excitation source was employed to image the UCNP-nanocomplex treated mice. The laser power density was ca. 0.2 W cm^{-2} during imaging. An 850 nm short-pass emission filter was applied to prevent the interference of excitation light to the CCD camera. T_1 and T_2 signals were analyzed by MicroMR-CA (Shanghai Niumag CO.,Ltd). MR imaging was accomplished with a 3 T clinical MRI scanner equipped with a special coil designed for small animal imaging.

Supporting Information

Supporting Information is available from the Wiley Online Library or from the author.

Acknowledgements

This work was partially supported by the National Basic Research Programs of China (973 Program) (2012CB932600, 2011CB911002), the National Natural Science Foundation of China (51222203, 51002100, 51132006), and a Project Funded by the Priority Academic Program Development (PAPD) of Jiangsu Higher Education Institutions.

Received: October 14, 2012
Revised: December 25, 2012
Published online: January 31, 2013

[1] C. A. Robertson, D. H. Evans, H. Abraharnse, *J. Photochem. Photobiol., B* **2009**, *96*, 1.
[2] A. P. Castano, P. Mroz, M. R. Hamblin, *Nat. Rev. Cancer* **2006**, *6*, 535.
[3] Y. M. Yang, Q. Shao, R. R. Deng, C. Wang, X. Teng, K. Cheng, Z. Cheng, L. Huang, Z. Liu, X. G. Liu, B. G. Xing, *Angew Chem., Int. Ed.* **2012**, *51*, 3125.
[4] J. Zhou, Z. Liu, F. Y. Li, *Chem. Soc. Rev.* **2012**, *41*, 1323.
[5] H. Y. Xing, W. B. Bu, S. J. Zhang, X. P. Zheng, M. Li, F. Chen, Q. J. He, L. P. Zhou, W. J. Peng, Y. Q. Hua, J. L. Shi, *Biomaterials* **2012**, *33*, 1079.
[6] X. J. Xue, F. Wang, X. G. Liu, *J. Mater. Chem.* **2011**, *21*, 13107.
[7] C. Wang, L. Cheng, Z. Liu, *Biomaterials* **2011**, *32*, 1110.
[8] L. Cheng, K. Yang, Y. Li, J. Chen, C. Wang, M. Shao, S. T. Lee, Z. Liu, *Angew. Chem., Int. Ed.* **2011**, *50*, 7385.
[9] F. Chen, W. B. Bu, S. J. Zhang, X. H. Liu, J. N. Liu, H. Y. Xing, Q. F. Xiao, L. P. Zhou, W. J. Peng, L. Z. Wang, J. L. Shi, *Adv. Funct. Mater.* **2011**, *21*, 4285.
[10] C. Bouzigues, T. Gacoin, A. Alexandrou, *ACS Nano* **2011**, *5*, 8488.
[11] F. Wang, Y. Han, C. S. Lim, Y. H. Lu, J. Wang, J. Xu, H. Y. Chen, C. Zhang, M. H. Hong, X. G. Liu, *Nature* **2010**, *463*, 1061.
[12] F. Wang, D. Banerjee, Y. Liu, X. Chen, X. Liu, *Analyst* **2010**, *135*, 1839.
[13] L. A. Cheng, K. Yang, S. A. Zhang, M. W. Shao, S. T. Lee, Z. A. Liu, *Nano Res.* **2010**, *3*, 722.
[14] D. K. Chatterjee, M. K. Gnanasammandhan, Y. Zhang, *Small* **2010**, *6*, 2781.
[15] M. Nyk, R. Kumar, T. Y. Ohulchanskyy, E. J. Bergey, P. N. Prasad, *Nano Lett.* **2008**, *8*, 3834.
[16] F. Zhang, G. B. Braun, A. Pallaoro, Y. C. Zhang, Y. F. Shi, D. X. Cui, M. Moskovits, D. Y. Zhao, G. D. Stucky, *Nano Lett.* **2012**, *12*, 61.
[17] C. Wang, L. Cheng, Z. Liu, *Ther. Delivery* **2011**, *2*, 1235.
[18] X. F. Qiao, J. C. Zhou, J. W. Xiao, Y. F. Wang, L. D. Sun, C. H. Yan, *Nanoscale* **2012**, *4*, 4611.
[19] C. Wang, L. Cheng, H. Xu, Z. Liu, *Biomaterials* **2012**, *33*, 4872.
[20] M. K. G. Jayakumar, N. M. Idris, Y. Zhang, *Proc. Natl. Acad. Sci. USA* **2012**, *109*, 8483.
[21] J. Wang, F. Wang, C. Wang, Z. Liu, X. Liu, *Angew. Chem., Int. Ed.* **2011**, *50*, 10369.
[22] Q. Liu, Y. Sun, T. S. Yang, W. Feng, C. G. Li, F. Y. Li, *J. Am. Chem. Soc.* **2011**, *133*, 17122.
[23] H. C. Guo, H. S. Qian, N. M. Idris, Y. Zhang, *Nanomed.: Nanotechnol. Biol. Med.* **2010**, *6*, 486.
[24] C. Wang, H. Tao, L. Cheng, Z. Liu, *Biomaterials* **2011**, *32*, 6145.
[25] P. Zhang, W. Steelant, M. Kumar, M. Scholfield, *J. Am. Chem. Soc.* **2007**, *129*, 4526.
[26] K. Liu, X. Liu, Q. Zeng, Y. Zhang, L. Tu, T. Liu, X. Kong, Y. Wang, F. Cao, S. A. Lambrechts, M. C. Aalders, H. Zhang, *ACS Nano* **2012**, *6*, 4054.
[27] N. M. Idris, M. K. Gnanasammandhan, J. Zhang, P. C. Ho, R. Mahendran, Y. Zhang, *Nat. Med.* **2012**, *18*, 1580.
[28] Y. I. Park, H. M. Kim, J. H. Kim, K. C. Moon, B. Yoo, K. T. Lee, N. Lee, Y. Choi, W. Park, D. Ling, K. Na, W. K. Moon, S. H. Choi, H. S. Park, S. Y. Yoon, Y. D. Suh, S. H. Lee, T. Hyeon, *Adv. Mater.* **2012**, *24*, 5755.
[29] H. S. Qian, H. C. Guo, P. C. Ho, R. Mahendran, Y. Zhang, *Small* **2009**, *5*, 2285.
[30] Y. Y. Yuan, C. Q. Mao, X. J. Du, J. Z. Du, F. Wang, J. Wang, *Adv. Mater.* **2012**, *24*, 5476.
[31] A. F. Radovic-Moreno, T. K. Lu, V. A. Puscasu, C. J. Yoon, R. Langer, O. C. Farokhzad, *ACS Nano* **2012**, *6*, 4279.
[32] H. P. Rim, K. H. Min, H. J. Lee, S. Y. Jeong, S. C. Lee, *Angew. Chem., Int. Ed.* **2011**, *50*, 8853.
[33] J. Z. Du, X. J. Du, C. Q. Mao, J. Wang, *J. Am. Chem. Soc.* **2011**, *133*, 17560.
[34] Y. L. Zhao, Z. Li, S. Kabehie, Y. Y. Botros, J. F. Stoddart, J. I. Zink, *J. Am. Chem. Soc.* **2010**, *132*, 13016.
[35] J. Z. Du, T. M. Sun, W. J. Song, J. Wu, J. Wang, *Angew. Chem., Int. Ed.* **2010**, *49*, 3621.
[36] C. C. Lee, J. A. MacKay, J. M. Frechet, F. C. Szoka, *Nat. Biotechnol.* **2005**, *23*, 1517.
[37] G. Tian, Z. Gu, L. Zhou, W. Yin, X. Liu, L. Yan, S. Jin, W. Ren, G. Xing, S. Li, Y. Zhao, *Adv. Mater.* **2012**, *24*, 1226.
[38] L. Xiong, T. Yang, Y. Yang, C. Xu, F. Li, *Biomaterials* **2010**, *31*, 7078.
[39] S. J. Jackson, R. Hussey, M. A. Jansen, G. D. Merrifield, I. Marshall, A. MacLullich, J. L. W. Yau, T. Bast, *Behav. Brain Res.* **2011**, *216*, 293.
[40] A. Bertin, J. Steibel, A. I. Michou-Gallani, J. L. Gallani, D. Felder-Flesch, *Bioconjugate Chem.* **2009**, *20*, 760.